Neural Spike Train Synchronization Indices: Definitions, Interpretations, and Applications

David M. Halliday* , J. R. Rosenberg, P. Breeze, and B. A. Conway

***Abstract*—A comparison of previously defined spike train syncrhonization indices is undertaken within a stochastic point process framework. The second-order cumulant density (covariance density) is shown to be common to all the indices. Simulation studies were used to investigate the sampling variability of a single index based on the second-order cumulant. The simulations used a paired motoneurone model and a paired regular spiking cortical neurone model. The sampling variability of spike trains generated under identical conditions from the paired motoneurone model varied from 50% to 160% of the estimated value. On theoretical grounds, and on the basis of simulated data a rate dependence is present in all synchronization indices. The application of coherence and pooled coherence estimates to the issue of synchronization indices is considered. This alternative frequency domain approach allows an arbitrary number of spike train pairs to be evaluated for statistically significant differences, and combined into a single population measure. The pooled coherence framework allows pooled time domain measures to be derived, application of this to the simulated data is illustrated. Data from the cortical neurone model is generated over a wide range of firing rates (1–250 spikes/s). The pooled coherence framework correctly characterizes the sampling variability as not significant over this wide operating range. The broader applicability of this approach to multielectrode array data is briefly discussed.**

***Index Terms*—Coherence, cross-correlation, motor units, synchronization indices.**

I. Introduction

THE CROSS-CORRELATION histogram is one of the principal analytical tools used to detect and characterize correlated motor-unit discharges during voluntary contractions in man [9], [19], [20]. The investigation of motor unit synchrony, through the use of the cross-correlation histogram, provides the basis for inferring the properties of common inputs to pairs of motor-units based on measures of the peak [9], [21], and for quantifying and comparing the strengths of these inputs ([10] and [23] for further references and discussion). The various measures used to characterize this peak are referred to collectively as "synchronization indices." Although there is no agreed method of calculating a synchronization index all of the proposed measures are based on the assumption that the magnitude of the synchrony estimated from the cross-correlation histogram must be positively correlated with the strength of the common input. This is often defined in terms of the number of shared branches of common presynaptic fibers and the distribution of arrival times and amplitudes of the post-synaptic potentials arising from the common sources [35]. This report deals with two unresolved issues related to the use of synchronization indices: 1) rate dependency, and 2) sampling variability.

The question of any dependence of synchronization indices on the rate of discharge of the motor units has received considerable attention [10], [21], [33], [35], [45]. Such a dependence would have implications for the use of synchronization indices as measures of the strength of common inputs [9], [16], [46]. We define all the synchronization indices which have been proposed in the literature within a single unified theoretical framework of stochastic point processes. This makes explicit the relationship between all the synchronization indices, and clearly demonstrates a rate dependence in all of these proposed measures.

The issue of synchronization index sampling variability has received less attention. Comparison of different indices or drawing inferences based on an estimated value of a particular index requires knowledge of the sampling variability of the estimated index. The number of repeat experiments required to assess this variability is unlikely to be realizable under the usual conditions for motor unit and single unit recordings in humans and behaving animals where record lengths are necessarily limited by considerations of attention to the task and the possible effects of fatigue [25]. In this study a simulation approach was adopted to estimate the sampling variability of a single synchronization index. The simulation used a realistic paired motoneurone model, with shared synaptic input, to derive the sampling variability of a synchronization index under different input conditions. Results from the simulation study allow guidelines to be given for assessing the significance of changes in the value of an estimated index under identical input conditions.

The broader applicability of synchronization indices is explored through a second set of simulations, based on a regular spiking cortical neurone model [43], over a wide range of output firing rates, from 1 spike/s to 250 spikes/s.

The paper concludes by describing an alternative frequency domain approach to the construction of synchronization indices. This method, which is based on coherence and pooled coherence measures [3] is compared with the existing time domain approach. A frequency domain approach has a number of advantages, these include the ability to compare an arbitrary number

Manuscript received June 13, 2005; revised November 27, 2005. This work was supported by The Wellcome Trust and EPSRC under Grant GR/R12350/01. *Asterisk indicates corresponding author.*

*D. M. Halliday is with the Department of Electronics, University of York, York YO10 5DD, U.K. (e-mail: dh20@ohm.york.ac.uk).

J. R. Rosenberg is with the Division of Neuroscience and Biomedical Systems, University of Glasgow, Glasgow G12 8QQ, U.K.

P. Breeze is with the Department of Statistics, University of Glasgow, Glasgow G12 8QQ, U.K.

B. A. Conway is with the Bioengineering Unit, University of Strathclyde, Glasgow G4 0NW, U.K.

Digital Object Identifier 10.1109/TBME.2006.873392

of pairs of spike trains for statistically significant differences, and the ability to provide parameters (in time and frequency domain) which summarize the strength of correlation across several records.

II. Synchronization Indices Defined as Point Process Parameters

This section gives formal definitions and estimation procedures for time domain synchronization indices in terms of stochastic point process parameters. Spike trains are regarded as samples of stationary stochastic point processes [15], [28], [36]. A sample record from a spike train N_1 of duration T is denoted $N_1(T)$, where $N_1(T)$ gives the number of events (spikes) in the interval $(0, T]$, and T is the number of samples in the record. Differential increments of the process N_1 at time t are denoted by $dN_1(t)$, where $dN_1(t) = N_1(t+dt) - N_1(t)$ gives the number of events in the sampling interval dt. The point processes are assumed to be second-order stationary, and it is further assumed that differential increments well separated in time are only weakly dependent. The latter is referred to as a mixing condition [12], [13], and in practice is satisfied by most spike trains. Point processes are further assumed to be orderly, which implies that only one event (spike) will occur in each sampling interval. The assumption of orderliness is important in that it allows certain point process parameters to be interpreted either in terms of expected values or as probabilities [12], [18], [40].

Two simultaneously recorded spike trains may be referred to as a realization of a bivariate point process. Let $[N_1(t), N_2(t)]$ be such a bivariate point process with differential increments at time t given by $\{dN_1(t), dN_2(t)\}$. The *mean intensity* or *mean rate*, P_1, of process N_1 is defined as

$$E\{dN_1(t)\} = P_1 dt \tag{1}$$

where $E\{\cdot\}$ denotes the averaging operator or mathematical expectation of a random variable. Since the process is assumed to be orderly, P_1 may be interpreted as

$$P_1 = \lim_{dt \to 0} \text{Prob} \frac{\{N_1 \text{event in} (t, t+dt]\}}{dt}. \tag{2}$$

The mean intensity P_2 of N_2 is similarly defined. The mean intensity, P_1 is estimated as

$$\hat{P}_1 = \frac{N_1(T)}{T}. \tag{3}$$

The hat symbol "^" is used to indicate an estimate of a point process parameter. The *second-order product density* at lag u, $P_{12}(u)$, is defined as

$$E\{dN_1(t+u) dN_2(t)\} = P_{12}(u) du dt \tag{4}$$

which may be interpreted as shown in (5) at bottom of page. The second-order product densities $P_{11}(u)$ and $P_{22}(u)$ are defined as in (4) by making the appropriate changes in the subscripts. Since the processes are assumed to be mixing, the increments $dN_1(t+u)$ and $dN_2(t)$ will become independent as u becomes large. Therefore, the asymptotic distribution for the second-order product density, $P_{12}(u)$, is

$$\lim_{u \to \infty} P_{12}(u) = P_1 P_2. \tag{6}$$

The definition of the *second-order cumulant*, $q_{12}(u)$, is

$$q_{12}(u) = P_{12}(u) - P_1 P_2. \tag{7}$$

From (6) this quantity tends to zero as $|u| \to \infty$. Therefore the second-order cumulant may be interpreted as a covariance density

$$\text{cov}\{dN_1(t+u), dN_2(t)\} = q_{12}(u) du dt \tag{8}$$

where "cov" denotes covariance [11].

The above point process product and cumulant densities may be directly estimated from the cross-correlation histogram. Denote the set of spike times for N_1 by $\{r_i; i = 1, 2, \ldots, N_1(T)\}$ and those for N_2 as $\{t_k; k = 1, 2, \ldots, N_2(T)\}$ for a sample record of duration T. The cross-correlation histogram, $J_{12}^T(u)$, may be written as:

$$J_{12}^T(u) = \#\left\{(r_i, t_k), \text{ such that } u - \frac{h}{2} < r_i - t_k < u + \frac{h}{2}\right\} \tag{9}$$

where $\#\{A\}$ indicates "the number of events in the set A." For each pair of spikes (r_i, t_k), $J_{12}^T(u)$ counts the number of occurrences of interspike intervals of duration $r_i - t_k$ lying in a bin of width h centered at lag u Following [17] the expected value of the cross-correlation histogram is

$$E\left\{J_{12}^T(u)\right\} \approx P_{12}(u) h T \tag{10}$$

$$P_{12}(u) = \frac{\lim_{du, dt \to 0} \text{Prob}\{N_1 \text{ event in } (t+u, t+u+du] \text{ and } N_2 \text{ event in } (t, t+dt]\}}{du dt} \tag{5}$$

which shows the relation between the cross-correlation histogram and the second-order product density, and suggests the following approximately unbiased estimate for $P_{12}(u)$ as

$$\hat{P}_{12}(u) = \frac{J_{12}^{T}(u)}{hT}. \tag{11}$$

The second-order cumulant can be estimated as $\hat{q}_{12}(u) = \hat{P}_{12}(u) - \hat{P}_1\hat{P}_2$.

Two important concepts used in the definition of synchronization indices are "expected counts" and "extra counts," these are normally defined with respect to the cross-correlation histogram [38]. The number of expected counts in the cross-correlation histogram between two spike trains N_1 and N_2, denoted here as $C_{12}^{\exp}$, can be defined in terms of the expected value of the cross-correlation histogram for uncorrelated spike trains. For any given pair of spike trains, N_1 and N_2, the value of this can be defined as the constant

$$C_{12}^{\exp} = hTP_1P_2. \tag{12}$$

Extra counts is defined as the number of counts which exceeds those which occur by chance [38]. The number of extra counts, denoted as $C_{12}^{\text{ext}}(u)$, at a particular value of lag u, can be defined as

$$C_{12}^{\text{ext}}(u) = hTq_{12}(u). \tag{13}$$

The definition in terms of the second-order cumulant density, $q_{12}(u)$, follows from (7) and (10). Therefore, the concept of "extra counts" is directly proportional to the value of the cumulant density, $q_{12}(u)$, at a particular lag, u. Equations (12) and (13) give definitions of extra and expected counts in terms of formal point process parameters. Estimates of these can be constructed as $\hat{C}_{12}^{\exp} = hT\hat{P}_1\hat{P}_2$ and $\hat{C}_{12}^{\text{ext}}(u) = hT\hat{q}_{12}(u)$. Equations (1)–(13) provide a unified framework within which synchronization indices can be defined and discussed.

A number of different synchronization indices have been introduced in the literature, all of these are based on the concept of "extra counts" in the cross-correlation histogram, defined in (13). For each index two expressions are given below, a formal definition in terms of point process parameters, and a discrete estimation procedure, based on the estimated second-order cumulant density, $\hat{q}_{12}(u)$. The first synchronization index based on the cross-correlation histogram, k, [30], [38], [44] is the ratio of the peak in the cross-correlation histogram to the mean level of the histogram, defined and estimated as

$$k = \frac{\max_u\{C_{12}^{\text{ext}}(u)\} + C_{12}^{\exp}}{C_{12}^{\exp}}, \quad \hat{k} = 1 + \frac{\max_u\{\hat{q}_{12}(u)\}}{\hat{P}_1\hat{P}_2}. \tag{14}$$

In the case of uncorrelated spike trains, $k = 1$. On the assumption that using the area under the peak of the cross-correlation histogram would reduce the variability associated with trial by trial fluctuations of the peak magnitude, the synchronization index k' was proposed as the ratio of the number of counts in the bins within the peak to the number of counts that would be expected to occur if the two processes were independent [21]. This index can be defined and estimated as

$$k' = \frac{\int_a^b C_{12}^{\text{ext}}(u)du + (b-a)C_{12}^{\exp}}{(b-a)C_{12}^{\exp}}, \quad \hat{k}' = 1 + \frac{\sum_{u=a}^{b}\hat{q}_{12}(u)}{(b-a)\hat{P}_1\hat{P}_2}. \tag{15}$$

This index, like all subsequent indices, depends on the specification of the parameters a and b, which specify the width of the central peak in the cross-correlation histogram (see Fig. 1). For the discrete estimation in (15), the quantity $(b-a)$ is an integer specifying the number of bins in the central peak of the histogram.

The synchronization index denoted by E, was introduced in [19] and [20], as the total number of "extra counts" within the peak of the cross-correlation histogram relative to the total number of reference events. This can be defined and estimated as

$$E = \frac{\int_a^b C_{12}^{\text{ext}}(u)du}{\mathrm{N}_{\text{ref}}(T)}, \quad \hat{E} = \frac{h}{\hat{P}_{\text{ref}}}\sum_{u=a}^{b}\hat{q}_{12}(u) \tag{16}$$

where $N_{\text{ref}}(T)$ and $\hat{P}_{\text{ref}}$ are the number of events and estimated mean intensity of the spike train with the slower mean rate.

The synchronization index, S, introduced in [1] and applied in [10] is defined by these authors as the total number of "extra counts" in the cross-correlation histogram peak relative to the

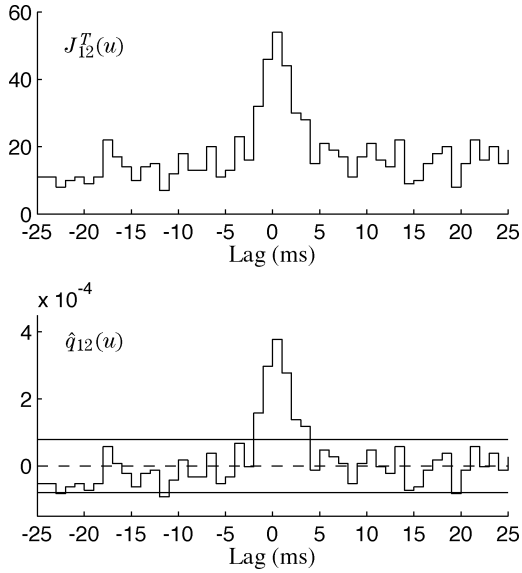

Fig. 1. Cross-correlation analysis of two spike trains generated by a paired motoneurone model with common and independent synaptic input. (top) cross-correlation histogram, $J_{12}^{T}(u)$, calculated using (9). (bottom) estimated cumulant density, $\hat{q}_{12}(u)$, calculated using (11) and (7). The solid horizontal lines are the estimated upper and lower 95% confidence limits, based on the assumption of independence. The limits of the central peak are taken as the interception of the cumulant with the upper 95% confidence limit, in this example these are $[-2, +4]$ ms, a total of 6 bins. Other parameters are $N_1(T) = 1269$, $N_2(T) = 1279$, $h = 1$ and $T = 10^5$.

total number of spikes in both the reference and response motor-unit spike trains. This can be defined and estimated as

$$S = \frac{\int_a^b C_{12}^{\text{ext}}(u)du}{N_1(T) + N_2(T)}, \quad \hat{S} = \frac{h}{\hat{P}_1 + \hat{P}_2} \sum_{u=a}^{b} \hat{q}_{12}(u). \tag{17}$$

The index denoted by SI was proposed in [32], and is defined as the ratio of "extra counts" in the histogram to the total number of pairs of counts in the entire cross-correlation histogram. This can be defined and estimated as

$$SI = \frac{\int_a^b C_{12}^{\text{ext}}(u)du}{N_1(T)N_2(T)}, \quad \widehat{SI} = \frac{h}{T\hat{P}_1\hat{P}_2} \sum_{u=a}^{b} \hat{q}_{12}(u). \tag{18}$$

The synchronization index referred to as the "common input synchronization" or CIS was introduced in [35]. This index is also based on the cross-correlation histogram, and in addition, depends on a model for a rhythmically discharging motoneurone [4], [5]. In its final form CIS is estimated by M/R_{s} where M is the number of counts in the cross-correlation histogram peak exceeding those expected by chance alone, and R_{s} is the duration of the record in seconds. This can be defined and estimated as

$$CIS = \frac{\int_a^b C_{12}^{\text{ext}}(u)du}{R_{\text{s}}}, \quad \widehat{CIS} = \frac{h}{dt} \sum_{u=a}^{b} \hat{q}_{12}(u). \tag{19}$$

The quantity dt is the sampling interval. The index β was introduced in [45]. The derivation of this index is given in terms of a joint peri stimulus time histogram (JPSTH, [2]), which involves splitting the complete record into a number of sections, each containing T' bins. The authors give an equivalent definition in terms of the cross-correlation histogram for the case of stationary spike trains. In the point process formalism this index can be defined and estimated as

$$\beta = \frac{\int_a^b C_{12}^{\text{ext}}(u)du + (b-a)C_{12}^{\text{exp}}}{T'}$$
$$\hat{\beta} = \frac{hT}{T'} \left(\sum_{u=a}^{b} \hat{q}_{12}(u) + (b-a)\hat{P}_1\hat{P}_2 \right). \tag{20}$$

The calculation of this index requires specification of the number of bins in the JPSTH. In [45], 100 ms sections containing 100 bins was used.

A number of common features are present in the synchronization indices defined in (14)–(20). All the indices depend on the second-order cumulant density, $q_{12}(u)$. The most common dependence is the integral of the cumulant across the central peak: $\int_a^b q_{12}(u)du$. The cumulant density is analogous to a covariance density (8). Therefore it will be sensitive to any changes in the variances of the individual spike trains. The principal determinant of the variance of a spike train is the mean intensity [8]. Thus any changes in the firing rate of a spike train will be reflected in the cumulant density and therefore in any synchronization index which depends on the cumulant density. Therefore, a rate dependency is implicit in all the synchronization indices defined herein.

With the exception of the index k, the integration over the second-order cumulant is common to all of the other synchronization indices. This integral is related to the index k' according to the relationship

$$\int_a^b q_{12}(u)du = (k'-1)(b-a)P_1P_2. \tag{21}$$

All the other indices (apart from k) can be expressed in terms of the index k' as $c_{\text{ind}}(k'-1)(b-a)$, ($c_{\text{ind}}k'(b-a)$ for the index β), where c_{ind} is a constant depending only on $N_1(T)$, $N_2(T)$, h, T, T' and dt.

The two main points of this section may be summarized as follows: (1) Synchronization indices other than the one proposed by [38] differ only by fixed scale factors, consequently given one, and the appropriate scale factors, all the others can be estimated. (2) All synchronization indices which are based on the second-order cumulant density, $q_{12}(u)$, have an implicit dependence on the mean rates of the motor units.

III. Sampling Variability of an Estimated Synchronization Index

The complexity of the expressions for the synchronization indices together with the need to estimate the width of the base of the peak in the second-order cumulant precludes a practical derivation of expressions for the sampling variability of the estimated synchronization indices. For example, to use Kendall's expression [41] for the approximate variance of k', the variance of the sum of the estimated values in the peak of the histogram, where the entries in this sum are not necessarily independent, and where the width of the peak is based on an estimate, and the covariance between this sum and the product of the estimated mean rates of the two processes would need to be specified. Simulation provides an important and widely used means of assessing the sampling variability of an estimated parameter in complex cases such as this.

In this section results are presented from simulation studies based on a motoneurone model and a regular spiking cortical neurone model [43]. A two cell configuration with common and independent synaptic input was used to generate paired spike train records for analysis. The equation describing the membrane potential for a single neurone, incorporating multiple synaptic inputs and afterhyperpolarization (AHP), is

$$C_m \frac{dV_m}{dt} = -I_{\text{leak}}(V_m) - \sum_{j=1}^{n} I_{\text{syn}}^{j}(t) - \sum_{i}^{k} I_{ahp}^{i}(t) \tag{22}$$

where C_m is the membrane capacitance, V_m the membrane potential, and $I_{\text{leak}}(V_m)$ the leakage current given by $(V_m - V_r)/R_m$ [24]. V_r and R_m represent the resting potential and membrane resistance, respectively. The synaptic current due to the jth synaptic input is $I_{\text{syn}}^{j}(t)$ with the summation in (22) over the total number of synaptic inputs, denoted by n. The synaptic current in response to a single input spike at time

zero was modeled by $I_{\rm syn}(t) = g_{\rm syn}(t)(V_m - V_{\rm syn})$, with $g_{\rm syn}(t)$ the time dependent conductance change, and $V_{\rm syn}$ the synaptic reversal potential. The time course of a single synaptic conductance change was represented by the alpha-function: $G_{\rm syn}(t/\tau_{\rm syn})\exp(-t/\tau_{\rm syn})$ [29], where $G_{\rm syn}$ is a constant scaling factor. $I_{ahp}(t)$ represents the output spike-triggered afterhyperpolarization current, where the summation for this term in (22) is over the number of output spikes, $I_{ahp}(t)$ was only included in the motoneurone model, the cortical neurone model incorporates a partial reset mechanism [43].

For the motoneurone model, $C_m = 1 \times 10^{-9}$ F, $R_m = 5 \times 10^6\ \Omega$ ($\tau_m = 5$ ms) and $V_r = -70$ mV. The time constant for the synaptic input, τ, was chosen to give an EPSP with a 10%–90% rise time of 1.8 ms and a half-width of 7.0 ms in relation to a membrane time constant of $\tau_m = 5$ ms. These values lie within the range used in [9]. The AHP was based on the model of [7] with a time constant of $\tau_{ahp} = 10$ ms.

For the cortical neurone model, $C_m = 0.5 \times 10^{-9}$ F, $R_m = 40 \times 10^6\ \Omega$, and $V_r = -74$ mV, giving a membrane time constant of $\tau_m = 5$ ms. The firing threshold was $V_{\rm thresh} = -54$ mV, and the partial reset after firing was $V_{reset} = -60$ mV. The model parameters were taken from [43], where parameters were chosen to match slice recordings of regular spiking cells. Both excitatory and inhibitory synaptic inputs were included. Excitatory synaptic conductances used an alpha function with a time constant of $\tau_{\rm syn} = 1$ ms, and a reversal potential of $V_{\rm syn} = 0$ mV. Inhibitory synaptic conductances used $\tau_{\rm syn} = 10$ ms and $V_{\rm syn} = -74$ mV. $G_{\rm syn}$ was set in both cases to give an EPSP and IPSP of magnitude $+370\ \mu$V and $-370\ \mu$V, respectively, both measured when injected current was used to elevate the membrane potential to $V_{\rm thresh}$.

Sampling Variability of Simulated Motoneurone Data:

Results from the motoneurone simulations are presented first. Each neurone received 200 synaptic inputs, 100 of which were shared between the two cells. The spike trains for the independent inputs to both motoneurones had exponentially distributed intervals. Two types of common input processes were used, one with an exponential distribution of interspike intervals and the other with a Gaussian distribution of intervals. All input spike trains were mutually independent. The mean intensity of common input spike trains was fixed at 30 spikes/s. The mean intensities for the independent inputs for each neurone were set separately to achieve the desired output rate.

The range of output firing rates was based on sustained firing rate ranges (6–18 spikes/s) commonly reported for human motor unit recordings [25], [35]. Simulations were divided into three different groups according to the output firing rate of one of the motoneurones, the reference rate, $P_{\rm ref}$. Three reference rates were selected, two at the extremes and one in the centre of this range. For each reference rate the output firing rate, or response rate $P_{\rm resp}$, of the second motoneurone was systematically adjusted to cover this range. The values for the reference rate and the range for the response rates for each of the three groups were: 1) 5 and 6–13; 2) 13 and 6–18; 3) 20 and 5–19; all values in spikes/s. Each group used thirteen different response rates to cover the ranges indicated. For each specific value of reference and response rate, seventy repeat runs were generated

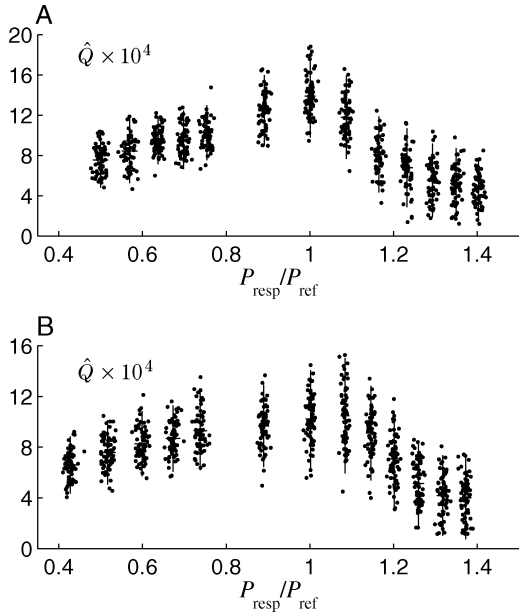

Fig. 2. Sampling variability of the synchronization index Q for (a) Poisson common input spike trains, and (b) Gaussian common input spike trains to the paired motoneurone model. Index values are plotted as a function of the ratio $P_{\rm resp}/P_{\rm ref}$, for thirteen fixed values of this ratio, with $P_{\rm ref} = 13$ spikes/s. Values of Q for each data set are indicated as dots, with 70 repeat runs at each value of $P_{\rm resp}$. Overlaid vertical lines indicate $\pm 2SD$ about the mean value of Q, horizontal lines indicate $\pm 2SD$ about the mean value of $P_{\rm resp}/P_{\rm ref}$.

to characterize the statistical distribution of the synchronization index, representing a total of 2730 separate simulations. A second set of 2730 simulations was also performed, in this case the ISI distribution of the common inputs was altered from Exponential (Poisson) to Gaussian, with a coefficient of variation (COV) of 0.1. All simulations generated 100 s of spike train data, output spike times were recorded with a sampling interval of 1 ms.

The second-order cumulant density, $q_{12}(u)$ is common to all the synchronization indices defined in the previous section. The present study therefore used as a comparative synchronization index the quantity $\sum_{u=a}^{b} q_{12}(u)$. For notational convenience we denote this quantity as Q. For the present series of simulations, which have fixed record lengths and fixed target mean rates, the synchronization indices defined above (apart from k, k', and β) have the form AQ, for a constant A. This simplification does not take into account the sampling variability of the firing rates during repeat runs (see Section V).

The estimation of Q requires limits for a and b to be defined. In the present study, these limits were taken as the intersection of the estimated cumulant density with the upper 95% confidence limit, based on the assumption of independence, which was approximated by the constant value $1.96\sqrt{\hat{P}_1\hat{P}_2/hT}$, [26]. This procedure avoids the need to estimate the limits a and b by visual inspection, and is part of a rigorous statistical analytical framework [26], [28] which can readily be incorporated into an algorithm, see Fig. 1. The sampling variability of the estimated index, $\hat{Q} = \sum_{u=a}^{b} \hat{q}_{12}(u)$ for the series of simulations with $P_{\rm ref} = 13$ spikes/s is illustrated in Fig. 2. This summarizes the results from 70 repeat runs at the 13 different ratios of $P_{\rm resp}/P_{\rm ref}$. Each dot in Fig. 2(a) and (b) represents the value of

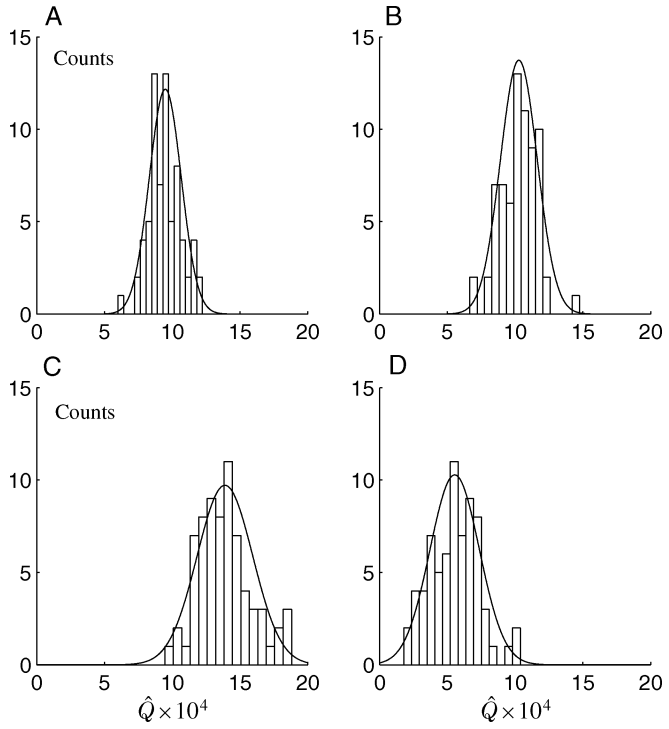

Fig. 3. Histograms of the distribution of values of $\hat{Q}$ for four fixed values of $P_{\rm resp}/P_{\rm ref}$ from Fig. 2(a). (a) $P_{\rm resp}/P_{\rm ref} = 0.64$. The mean and SD estimated from the histogram are 9.5, 1.2. (b) $P_{\rm resp}/P_{\rm ref} = 0.75$. Mean, SD are 10.3, 1.4. (c) $P_{\rm resp}/P_{\rm ref} = 1.00$. Mean, SD are 13.9, 2.0. (d) $P_{\rm resp}/P_{\rm ref} = 1.3$. Mean, SD are 5.5, 1.8. For all histograms $N = 70$. Solid curves are normal distributions based on the mean and SD estimated from the data.

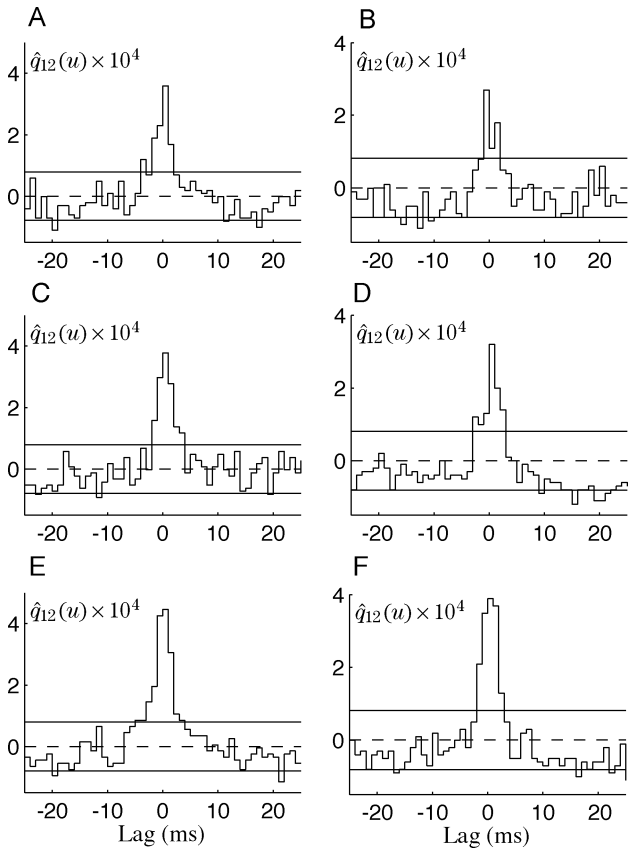

Fig. 4. Individual cumulant density estimates illustrating sampling variability in synchronization indices derived from the cross-correlation histogram for the paired motoneurone simulation. The individual plots show the (a) and (b) minimum, (c) and (d) median, and (e) and (f) maximum for the configuration in Fig. 2 with $P_{\rm resp}/P_{\rm ref} = 1$, with (a), (c), and (e) Poisson inputs and (b), (d), and (f) Gaussian inputs. Individual values of synchronization indices are: (a) $\hat{Q} = 9.46 \times 10^{-4}$, $\hat{k}' = 2.47$, $\hat{E} = 0.0747$, $\hat{S} = 0.0373$, $\widehat{SI} = 5.88 \times 10^{-10}$, and $\widehat{CIS} = 0.946$, with $N_1(T) = 1270$ and $N_2(T) = 1267$; (b) $\hat{Q} = 5.57 \times 10^{-4}$, $\hat{k}' = 2.09$, $\hat{E} = 0.0428$, $\hat{S} = 0.0213$, and $\widehat{SI} = 3.26 \times 10^{-10}$, $\widehat{CIS} = 0.557$, with $N_1(T) = 1313$ and $N_2(T) = 1302$; (c) $\hat{Q} = 1.37 \times 10^{-3}$, $\hat{k}' = 2.40$, $\hat{E} = 0.108$, $\hat{S} = 0.0536$, $\widehat{SI} = 8.42 \times 10^{-10}$, $\widehat{CIS} = 1.37$, with $N_1(T) = 1269$, and $N_2(T) = 1279$; (d) $\hat{Q} = 1.01 \times 10^{-3}$, $\hat{k}' = 1.99$, $\hat{E} = 0.0777$, $\hat{S} = 0.0387$, $\widehat{SI} = 5.93 \times 10^{-10}$, and $\widehat{CIS} = 1.01$, with $N_1(T) = 1298$ and $N_2(T) = 1311$; (e) $\hat{Q} = 1.88 \times 10^{-3}$, $\hat{k}' = 2.27$, $\hat{E} = 0.147$, $\hat{S} = 0.0734$, $\widehat{SI} = 1.14 \times 10^{-9}$, and $\widehat{CIS} = 1.88$, with $N_1(T) = 1281$ and $N_2(T) = 1283$; (f) $\hat{Q} = 1.45 \times 10^{-3}$, $\hat{k}' = 2.69$, $\hat{E} = 0.111$, $\hat{S} = 0.0553$, $\widehat{SI} = 8.46 \times 10^{-10}$, and $\widehat{CIS} = 1.45$, with $N_1(T) = 1306$ and $N_2(T) = 1308$. In all cases $h = 1.0$ and $T = 10^5$

$\hat{Q}$ for one simulation run, plotted against the ratio $P_{\rm resp}/P_{\rm ref}$. The superimposed horizontal and vertical lines represent $\pm 2SD$ about the estimated mean, the 13 vertical lines give an indication of the spread of Q values for each value of $P_{\rm resp}$ that results purely from the sampling variability. The horizontal lines show the variability in the value of the ratio $P_{\rm resp}/P_{\rm ref}$ obtained with repeat runs under identical input conditions.

The distribution of the index Q is explored in Fig. 3, which illustrates histograms of $\hat{Q}$ values for 4 fixed values of $P_{\rm resp}$ from the series of simulations with Poisson common input spike trains in Fig. 2(a). Overlaid on each histogram is a normal pdf with mean and SD estimated from the data, and amplitude scaled to match each histogram. These histograms are well fitted with a normal distribution, thus the magnitude of the vertical lines in Fig. 2(a) and (b), which indicate $\pm 2SD$ can be used practically as a measure of the sampling variability of the index Q.

One approach to quantify the sampling variability of the index is to express the range of sampling variability as a percentage of the mean value, this quantifies the length of the vertical lines in Fig. 2 (see, also, Fig. 5) as a percentage of the mean index in each set. The ratio $4SD/\overline{Q}$ is used, where $\overline{Q}$ is the mean value of the estimated index, $\hat{Q}$ over the 70 repeat runs at each of the 13 values of $P_{\rm resp}$. This gives a range of values of 0.5–1.3 for the Poisson common input spike trains, and 0.6–1.6 for the Gaussian common input spike train. Thus the sampling variability of the index Q lies between 50% and 160% of the estimated value of the index. To a first approximation, ignoring the firing rate sampling variability with repeat runs, these conclusions also apply to the indices E, S, SI, and CIS defined in the previous section. Fig. 4 illustrates variations in the shape of $\hat{q}_{12}(u)$ that occur with repeat runs. The estimated cumulant density functions correspond to the median and extremes of the index Q for Poisson and Gaussian common input spikes trains. The changes in the shape of the central peak in this figure, and the indices derived from these (see figure legend), are entirely accounted for by the sampling variability of the indices. Fig. 5 summarizes the results of the simulations for the two other reference rates used, $P_{\rm ref} = 5$ spikes/s [Fig. 5(a) and (b)], and $P_{\rm ref} = 20$ spikes/s [Fig. 5(c) and (d)], these demonstrate a similar level of variability. The ratio $4SD/\overline{Q}$, ranges from 0.5–1.4 for $P_{\rm ref} = 5$ spikes/s, and 0.7–1.1 for $P_{\rm ref} = 20$ spikes/s. Two

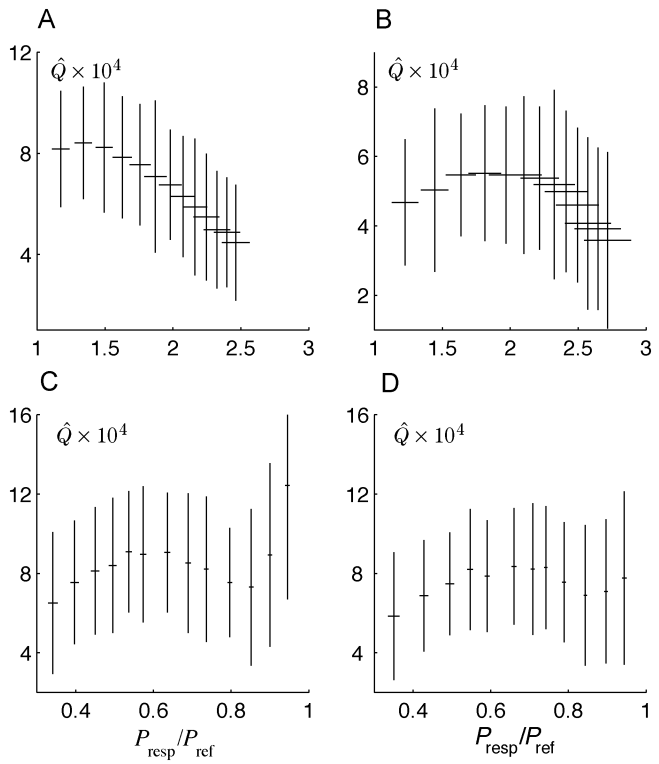

Fig. 5. Sampling variability of the synchronization index Q from the paired motoneurone model for (a) and (b) $P_{\text{ref}} = 5$ spikes/s, and (c) and (d) $P_{\text{ref}} = 20$ spikes/s. (a) and (c) have Poisson common input spike trains, (b) and (d) have Gaussian common input spike trains to the paired motoneurone model. Format of plots is identical to that in Fig. 2(c) and (d).

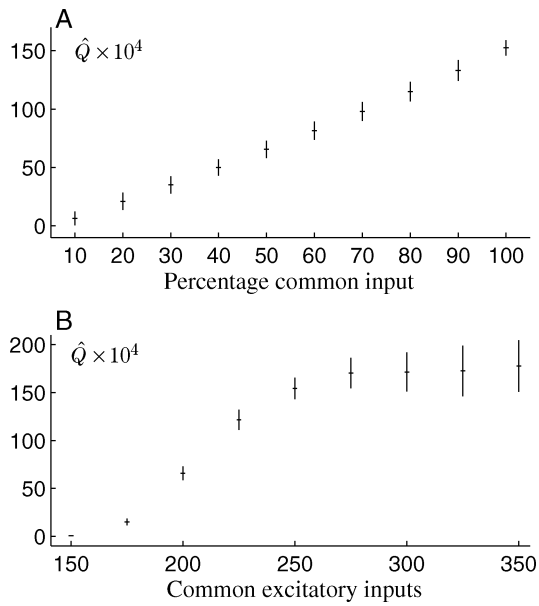

Fig. 6. Sampling variability of the synchronization index Q from the paired cortical neurone model for (a) Fixed number of 400 excitatory inputs per neurone, with the percentage of common inputs varied from 10% to 100%. (b) Fixed percentage of common excitatory inputs (50%), with the number of common inputs varied from 150 to 350. The first order statistics for the output discharges in the 9 groups, spikes/s (COV), are 0.98(1.00), 9.4(1.04), 32.7(0.92), 67(0.76), 106(0.63), 147(0.53), 187(0.46), 227(0.41), and 267(0.37). Vertical lines in (a) and (b) indicate $\pm 2SD$ about the mean value of Q, horizontal are used to indicate the mean for each group.

main conclusions can be drawn from the simulations results illustrated in Figs. 2–5. The estimated synchronization index exhibits a similar range of variability across the range of firing rates typically found in motor unit recordings. Quantifying this variability as a percentage of the the mean index gives a range of 50%–160%.

Sampling Variability of Simulated Cortical Neurone Data:

The second set of simulations is based on the regular spiking cortical neurone described above. Two different input scenarios were investigated. In the first scenario the total number of synaptic inputs remained fixed, and the percentage of common inputs was varied systematically from 10% to 100%. Each cell received 100 inhibitory inputs and 400 excitatory inputs, all inputs were driven by independent Poisson spike trains of rate 10 spikes/s. The inhibitory inputs were always applied independently to each cell, only excitation was shared between the two cells. The results from this configuration are illustrated in Fig. 6(a), the vertical lines indicate $\pm 2SD$ about the estimated mean index at each percentage of common inputs, derived from 70 repeat runs. The mean output rate and COV across all 10 groups, was 32.7 spikes/s, and 0.92, respectively. The second scenario used a fixed percentage of common excitatory input (50%), however the numbers of common excitatory inputs was varied from 150 to 350. Both cells also independently received 100 inhibitory inputs. Excitatory and inhibitory firing rates were 10 spikes/s. The output firing rate of the two cortical neurons varied from 1 spike/s (150 common inputs) to 267 spikes/s (350 common inputs). The vertical lines in Fig. 6(b) indicate $\pm 2SD$ about the estimated mean index for each group, derived from 70 repeat runs. The horizontal lines in Fig. 6 serve only to indicate the mean value for each group, (they do not indicate any variability as in Figs. 2 and 5).

Quantitatively, the results in Fig. 6 can be summarized using the same ratio as above. In Fig. 6(a), the ratio $4SD/\overline{Q}$ decreases monotonically from 180% to 9% as the percentage of common input increases. This reflects an increase in the mean value of index with increasing percentage of common input, whereas the variability in the estimated index is relatively constant. In Fig. 6(b) the ratio ranges from 15% to 49% (not including the first point), as both the mean value of the index and the variability increase as the number of common inputs increases. Fig. 6(b) also suggests a strong rate dependence in the value of the synchronization index, the mean index increasing as the mean output firing rate of the two neurones increases. The synchronization index sampling variability for the cortical neurone model is quantitatively similar to that for the paired motoneurone model, which suggests the patterns of sampling variability illustrated in Figs. 2, 5, and 6 is representative across a wide range of neural spike train data. The next section describes the application of an alternative frequency domain approach which can deal with this sampling variability in a rigorous statistical manner.

IV. Frequency Domain Approach for Comparing Synchronization Indices—Pooled Coherence

There has been an increased use of Fourier-based methods for defining measures of association between neuronal signals

[28], [36]. One frequency domain measure of association, the coherence, provides a normative measure of the strength of association on a scale from zero to one. The coherence can be defined in terms of the magnitude squared of the cross-spectrum between the two processes, which in turn can be obtained from the Fourier transform of the second-order cumulant density, (8). Therefore, the second-order cumulant density and the coherence provide alternative measures of association between two spike trains. The technique of pooled coherence was introduced in [3] as a method of pooling and comparing independent coherence estimates. Here, it is proposed to use pooled coherence as an alternative frequency domain synchronization index. A pooled coherence analysis includes two components. These are the construction of a pooled estimate across a number of independent coherence estimates, and a χ^2 statistic which is used to test the *null* hypothesis that all the individual coherence estimates have a common mean at each frequency. The method used to calculate the pooled coherence and the chi squared statistic is given in [3]. In addition, the pooled coherence framework allows pooled cumulant density estimates to be constructed, these provide a population time domain measure of association.

Fig. 7 presents a pooled coherence analysis applied to the simulated motoneurone data. Fig. 7(a) illustrates the coherence estimates corresponding to the three cumulant density estimates for Gaussian common inputs shown in Fig. 4 (right column). Overlaid in bold is the pooled coherence estimate for all 70 records in this group. The pooled and ordinary coherence estimates are all similar in form. As well as providing a normative value for the strength of association, the coherence estimates also show that this correlation is centered about 30 Hz, the frequency of the common Gaussian inputs in this case. Fig. 7(b) shows the χ^2 extended difference of coherence test and Fig. 7(c) the pooled cumulant density for all 70 simulations in this particular set of simulations. The χ^2 test statistic does not assume any significant values, thus the hypothesis of equal coherence estimates is accepted in this case. Therefore, the pooled coherence analysis indicates no significant differences in the strength of correlation between any of the 70 records, as expected. The pooled coherence analysis quantifies within a theoretical framework the sampling variability present in the individual cumulant [Fig. 4(b), (d), and (f)] and coherence [Fig. 6(a)] estimates as acceptable within the null hypothesis of equal strength of correlation between the 70 pairs of spike trains. Fig. 7(c) illustrates the pooled cumulant density estimate for all 70 simulations. From this a single representative value of $\hat{Q}$ can be derived (see legend). The significant symmetrical negative values in Fig. 7(c) are due to the periodic modulation of the cumulant which results from the periodic output discharge of the motoneurone model. Similar features are seen in experimental data [25].

Fig. 8 present the same analysis applied to data from the cortical neurone model. The pooled analysis is applied to the centre group of data in Fig. 6(b), where each neurone has 250 shared and 250 independent excitatory synaptic inputs. The three ordinary coherence estimates in Fig. 8(a) are for spike train pairs with the minimum, median, and maximum values of $\hat{Q}$, the bold line is the pooled coherence estimate for all 70 spike train pairs in the group. For this set of data the coherence is broad band in nature, reflecting the random discharge of the common input

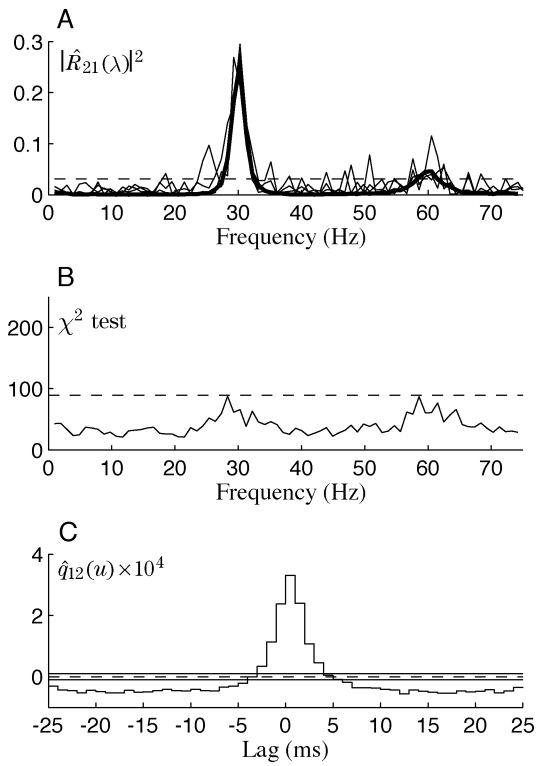

Fig. 7. Pooled coherence analysis for 70 pairs of spike trains with common Gaussian common inputs from the paired motoneurone simulation, $P_{\mathrm{ref}} = 13\ \mathrm{spikes/s}$ and $P_{\mathrm{resp}}/P_{\mathrm{ref}} = 1$. (a) Individual coherence estimates (normal lines), $|\hat{R}_{21}(\lambda)|^2$, corresponding to cumulant density estimates in Fig. 4(b), (d), and (f), respectively. Horizontal dashed line is upper 95% confidence limit based on the assumption of independence. The bold line is the Pooled coherence estimate across all 70 records (the upper 95% limit for this estimate is 4.4×10^{-4}). (b) Computed value of χ^2 test statistic across the 70 records. The horizontal dashed line is the upper 95% confidence limit under the *null* hypothesis of equal coherences, $(\chi^2_{(0.05;69)} = 98.4)$. (c) Pooled cumulant density derived from pooled cross spectrum. Solid horizontal lines are 95% confidence limits under the assumption of independence. The value of synchronization index derived from this is $\hat{Q} = 1.11 \times 10^{-3}$, with $N_1(T) = 90\,772$, $N_2(T) = 90\,964$, $T = 6\,952\,960$, and $h = 1$ in the pooled analysis.

spike trains. As in Fig. 7, there is no evidence in the χ^2 test statistic [Fig. 8(b)] of any statistically significant differences in the 70 coherence estimates in the group. Fig. 8(c) illustrates the pooled cumulant estimate for the 70 records, a single summary value of $\hat{Q}$ is given in the figure legend. Similar conclusions result from a pooled coherence analysis of all 19 groups of data in Fig. 6. A pooled coherence approach to synchronization indices appears to have broad applicability to a range of neural spike train data.

V. Discussion

The definition, application and interpretation of neural spike train synchronization indices have been reviewed, within a stochastic point process framework. The key concept in the definition of all the synchronization indices reviewed is that of "extra counts", this was shown to be directly related to the second-order cumulant density function, $q_{12}(u)$. The majority of indices involve the summation of extra counts in a central peak in the cross-correlation histogram. The index Q defined as $Q = \sum_{u=a}^{b} q_{12}(u)$ was used as a comparative time domain synchronization index. All previously defined indices can be written as

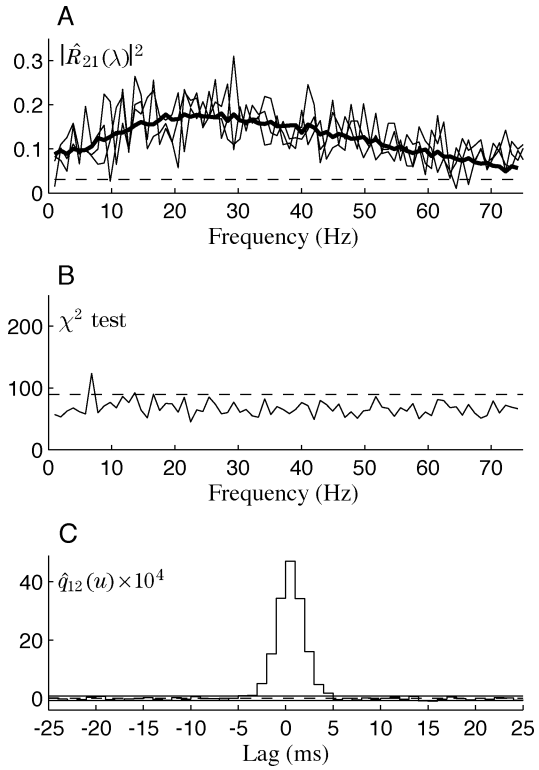

Fig. 8. Pooled coherence analysis for 70 pairs of spike trains with Poisson common inputs from the paired cortical neurone simulation, with 250 common excitatory inputs. (a) Individual coherence estimates (normal lines), $|\hat{R}_{21}(\lambda)|^2$, corresponding to the minimum, median, and maximum values of the index $\hat{Q}$ across the 70 records. Horizontal dashed line is upper 95% confidence limit based on the assumption of independence. The bold line is the Pooled coherence estimate across all 70 records (the upper 95% limit for this estimate is 4.4×10^{-4}). (b) Computed value of χ^2 test statistic across the 70 records. The horizontal dashed line is the upper 95% confidence limit under the *null* hypothesis of equal coherences, ($\chi^2_{(0.05;69)} = 98.4$). (c) Pooled cumulant density derived from pooled cross spectrum. Solid horizontal lines are 95% confidence limits under the assumption of independence. The value of synchronization index derived from this is $\hat{Q} = 16.1 \times 10^{-3}$, with $N_1(T) = 739\,667$, $N_2(T) = 739\,620$, $T = 6\,952\,960$, and $h = 1$ in the pooled analysis.

$AQ + B$ where A and B are constants depending on the values $N_1(T)$, $N_2(T)$, h, T, T' and dt. Therefore, the properties of the second-order cumulant density, or cross covariance function $q_{12}(u)$ [11], [36], are central to our treatment of time and frequency domain synchronization indices.

In our comparative framework, we have introduced a simple, statistically rigorous method of determining the width of the central peak by using an upper 95% confidence limit on the estimated cumulant density function. This avoids the need to determine the limits through visual inspection, and can easily be incorporated into an algorithm to automatically calculate the value of a synchronization index. The definition of the central peak was taken as the sum of the estimated cumulant density over the limits, a and b obtained using this procedure. An alternative approach, consistent with accepted statistical practice, would be to take the area above the 95% confidence limit. The present approach, however, is consistent with previous definitions of synchronization indices. Repeating the analysis using an index based on the area above the 95% confidence limit gives similar quantitative results to those reported here (not shown). Both approaches provide an objective, repeatable procedure for defining the extent of any central peak.

An important question is to what extent the sampling variability of estimates of the index Q is representative of the sampling variability of previously defined indices. If the sampling variability of the target firing rates is ignored then examination of the sampling variability of Q can be used as an indicator of the sampling variability of these indices. Thus, to a first approximation, the sampling variability illustrated in Figs. 2, 5, and 6 also applies to the other indices. However, it is important to note that this ignores the sampling variability of the individual firing rates included in the definitions of the indices. A more complete description in the case of k', E, S, and SI would involve the sampling variability of the ratio of two random variates. In the case of the index β the appropriate expression would include the sum of two random variates, the second term depending on the product of two random variates describing the firing rates. Expressing the sampling variability of Q as the ratio $4SD/\overline{Q}$ gave a range of values from 0.5–1.6 for the range of firing rates examined in the simulated motoneurone data. Figs. 2 and 5 can be used to provide indicative sampling variabilities for the comparison of individual time domain indices constructed from motor unit data with firing rates which match those illustrated.

The statistics of the input process to the paired motoneurone model, Gaussian or Poisson spike trains, does not have a significant effect on the sampling variability of the estimated synchronization index. However, the value of Q was, in general, larger with Poisson common inputs than with Gaussian common inputs. The simulation results also suggest the presence of a rate dependence in synchronization indices based on Q. For the set of simulation results shown in Fig. 2 ($P_{\mathrm{ref}} = 13$ spikes/s) the mean value is greatest when the ratio $P_{\mathrm{resp}}/P_{\mathrm{ref}}$ is closest to 1.0. There is a suggestion of a similar effect in the simulation results in Fig. 5, $P_{\mathrm{ref}} = 5$ and $P_{\mathrm{ref}} = 20$. The cortical neurone data in Fig. 6(b), which has a fixed percentage of common excitatory input, exhibits a strong rate dependency with increasing numbers of common inputs Therefore, on both theoretical grounds, see above, and on the basis of simulation, synchronization indices appear to exhibit a rate dependency. This finding is in contrast to [35] and [45].

The present report has in addition investigated the use of a frequency domain approach to neural spike train synchronization indices. A frequency domain approach based on pooled coherence has several advantages over a direct time domain approach. Since individual coherence estimates provide a normative measure of association, then the framework allows direct statistical comparison of two (or more) coherence estimates. The mathematical equivalence of the cumulant density function, $q_{12}(u)$, and the cross spectrum allow a pooled cumulant density estimate to be constructed from the pooled cross spectrum, this can in turn be used to construct a population synchronization index summarizing the strength of correlation across several records (Figs. 7 and 8). The χ^2 extended difference of coherence test provides a summary statistic describing any significant differences in the correlation between different reocrds. Details of the pooled coherence framework are in [3]. Further comments on the usage of pooled coherence are in [6],

[27]. The issue of preprocessing of spike trains regarding alignment of the central peak prior to pooled analysis is discussed in [25].

The individual coherence estimates in Fig. 7(a) are estimated from the same data sets as the cumulant density estimates in Fig. 4 (right column). The individual examples in Fig. 4 were chosen to illustrate the two extremes and the median value of $\hat{Q}$ obtained across the 70 repeat trials. It is striking that the individual coherence estimates (corresponding to these extremes in the time domain representations) are remarkably similar in appearance. Visual inspection of the three individual coherence estimates in Fig. 7(a) would probably lead to the conclusion of no significant differences in the correlation structure in the three pairs of spike trains, as verified by the pooled analysis. Similar conclusions can be drawn from the ordinary coherence estimates for the cortical neurone data in Fig. 8(a), which represent the two extremes and median value of $\hat{Q}$ across the 70 repeats. The cumulant density and cross spectrum (from which the coherence is constructed) are mathematically equivalent, through the use of the Fourier transform. This mathematical equivalence does not, however, imply an equivalence of representation [36]. It has been suggested that coherence analysis between pairs of motor unit recordings may be more appropriate for highlighting changes in the common input during voluntary contractions [39]. The present results suggest a frequency domain approach provides a more flexible and rigorous approach to neural spike train synchronization indices.

The primary focus of this report has been on synchronization indices applied to paired motor unit data. The inclusion of a regular spiking cortical neurone model has demonstrated the broader applicability of a frequency domain approach to measures of synchronization. Recent developments in multielectrode recording techniques can generate large numbers of simultaneously recorded spike trains from *in vivo* and *in vitro* [14], [31], [34] and cultured neurone preparations [42]. The techniques outlined above may be suitable for analysis of neural synchronization across these different preparations.

REFERENCES

[1] L. Adams, A. K. Datta, and A. Guz, "Synchronization of motor-unit firing during different respiratory and postural tasks in human sternocleidomastoid muscle," *J. Physiol.*, vol. 413, pp. 213–231, 1989.

[2] A. M. H. J. Aertsen, G. L. Gerstein, M. K. Habib, and G. Palm, "Dynamics of neuronal firing correlation: modulation of effective connectivity," *J. Neurophysiol.*, vol. 61, pp. 900–917, 1989.

[3] A. M. Amjad, D. M. Halliday, J. R. Rosenberg, and B. A. Conway, "An extended difference of coherence test for comparing and combining several independent coherence estimates—theory and application to the study of motor units and physiological tremor," *J. Neurosci. Meth.*, vol. 73, pp. 69–79, 1997.

[4] P. Ashby and D. Zilm, "Relationship between EPSP shape and cross-correlation profile explored by computer simulation for studies on human motoneurones," *Exp. Brain Res.*, vol. 47, pp. 33–40, 1982.

[5] ——, "Characteristics of postsynaptic potentials produced in single motoneurones by homonymous Group I volleys," *Exp. Brain Res.*, vol. 4, pp. 41–48, 1982.

[6] S. N. Baker, "Pooled coherence, can overestimate the significance of coupling in the presence of inter-experiment variability," *J. Neurosci. Meth.*, vol. 96, p. 1712, 2000.

[7] F. Baldissera and B. Gustafsson, "After hyperpolarization conductance time course in lumbar motoneurones of the cat," *Acta Physiol. Scand*, vol. 91, pp. 512–527, 1974.

[8] M. S. Bartlett, "The spectral analysis of point processes," *J. the Roy. Statist. Soc.*, vol. B25, pp. 264–280, 1963.

[9] F. D. Bremner, J. R. Baker, and J. A. Stephens, "Correlation between discharges of motor units recorded from the same and from different finger muscles in man," *J. Physiol.*, vol. 432, pp. 355–380, 1991.

[10] ——, "Variation in the degree of synchrony exhibited by motor-units lying in different finger muscles," *J. Physiol.*, vol. 432, pp. 381–399, 1991.

[11] D. R. Brillinger, "The identification of point process systems," *Ann. Probability*, vol. 3, pp. 909–929, 1975.

[12] ——, *Statistical inference for stationary point processes* (in Stochastic Processes and Related Topics)M. I. Puri, Ed. New York: Academic, 1975, pp. 57–79.

[13] ——, "Estimation of second-order intensities of a bivariate stationary point process," *J. Roy. Statist. Soc.*, vol. B38, pp. 60–66, 1976.

[14] A.-H. Chen, Y. Zhou, H.-Q. Gong, and P.-J. Liang, "Firing rates and dynamic correlated activities of ganglion cells both contribute to retinal information processing," *Brain Res.*, vol. 1017, pp. 13–20, 2004.

[15] B. A. Conway, D. M. Halliday, and J. R. Rosenberg, "Detection of weak synaptic interactions between single Ia afferent and motor-unit spike trains in the decerebrate cat," *J. Physiol.*, vol. 471, pp. 379–409, 1993.

[16] T. C. Cope, E. E. Fetz, and M. Matsumura, "Cross-correlation assessment of synaptic strength of single Ia fiber connections with triceps surae motoneurones in cats," *J. Physiol.*, vol. 390, pp. 161–188, 1987.

[17] D. R. Cox, "On the estimation of the intensity function of a stationary point process," *J. Roy. Statist. Soc.*, vol. B27, pp. 322–327, 1965.

[18] D. R. Cox and P. A. W. Lewis, "Multiple point processes," in *Proc. 6th Berkeley Symp. Mathematics, Statistics and Probability*, L. M. LeCam, J. Neyman, and E. L. Scott, Eds., Berkeley, 1972, vol. 3, pp. 401–448.

[19] A. K. Datta, S. F. Farmer, and J. A. Stephens, "Central nervous pathways underlying synchronization in human motor-unit firing studied during voluntary contractions," *J. Physiol.*, vol. 432, pp. 401–425, 1991.

[20] A. K. Datta and J. A. Stephens, "Synchronization of motor-unit activity during voluntary contractons in man," *J. Physiol.*, vol. 422, pp. 397–419, 1990.

[21] P. H. Ellaway and K. S. K. Murthy, "The origins and characteristics of cross-correlated activity between γ-motoneurones in the cat," *Quarter. J. Exp. Physiol.*, vol. 70, pp. 219–232, 1985.

[22] ——, "The source and distribution of short-term synchrony between γ-motoneurones in the cat," *Quarter. J. Exp. Physiol.*, vol. 70, pp. 233–247, 1985b.

[23] S. F. Farmer, F. D. Bremner, D. M. Halliday, J. R. Rosenberg, and J. A. Stephens, "The frequency content of common synaptic inputs to motoneurones studied during voluntary isometric contractions in man," *J. Physiol.*, vol. 470, pp. 127–155, 1993.

[24] P. A. Getting, "Reconstruction of small neural networks," in *Methods in Neuronal Modeling*, C. Koch and I. Segev, Eds., 1st ed. Cambridge, MA, USA: MIT Press, 1989, pp. 177–194.

[25] D. M. Halliday, B. A. Conway, S. F. Farmer, and J. R. Rosenberg, "Load-independent contributions from motor-unit synchronization to human physiological tremor," *J. Neurophysiol.*, vol. 82, pp. 664–675, 1999.

[26] D. M. Halliday and J. R. Rosenberg, "Time and frequency domain analysis of spike train and time series data," in *Modern Techniques in Neuroscience Research*, U. Windhorst and H. Johansson, Eds. Berlin, Germany: Springer-Verlag, 1999, ch. 18, pp. 503–543.

[27] ——, "On the application, estimation and interpretation of coherence and pooled coherence," *J. Neurosci. Meth.*, vol. 100, pp. 173–174, 2000.

[28] D. M. Halliday, J. R. Rosenberg, A. M. Amjad, P. Breeze, B. A. Conway, and S. F. Farmer, "A framework for the analysis of mixed time series/point process data—theory and application to the study of physiological tremor, single motor unit discharges and electromyograms," *Prog. Biophys. Mol. Biol.*, vol. 64, pp. 237–278, 1995.

[29] J. J. B. Jack, D. Noble, and R. W. Tsien, *Electric Current Flow in Excitable Cells*. Oxford, U.K.: Clarenden, 1975.

[30] Kirkwood and T. A. Sears, "The synaptic connections to intercostal motoneurones as revealed by the average common excitation potential," *J. Physiol.*, vol. 275, pp. 103–134, 1978.

[31] M. Laubach, J. Wessberg, and M. A. L. Nicolelis, "Cortical ensemble activity increasingly predicts behavior outcomes during learning of a motor task," *Nature*, vol. 405, pp. 567–571, 2000.

[32] E. L. Logigian, M. M. Wierzbicka, F. Bruyninckx, A. W. Wiegner, B. T. Shahani, and R. R. Young, "Motor-unit synchronization in physiologic, enhanced physiologic, and voluntary tremor," *Ann. Neurol.*, vol. 23, pp. 242–250, 1988.

[33] P. B. C. Matthews, "Relationship of firing intervals of human motor units to the trajectory of post-spike after-hyperpolarization and synaptic noise," *J. Physiol.*, vol. 492, pp. 597–628, 1996.
[34] M. A. L. Nicolelis and S. Ribeiro, "Multielectrode recordings: the next steps," *Curr. Opinion Neurobiol.*, vol. 12, pp. 602–606, 2002.
[35] M. A. Nordstrom, A. J. Fuglevand, and R. M. Enoka, "Estimating the strength of common input to human motoneurones from the cross-correlogram," *J. Physiol.*, vol. 453, pp. 547–574, 1992.
[36] J. R. Rosenberg, A. M. Amjad, P. Breeze, D. R. Brillinger, and D. M. Halliday, "The Fourier approach to the identification of functional coupling between neuronal spike trains," *Prog. Biophys. Mol. Biol.*, vol. 53, pp. 1–31, 1989.
[37] J. R. Rosenberg, D. M. Halliday, P. Breeze, and B. A. Conway, "Identification of patterns of neuronal connectivity—partial spectra, partial coherence, and neuronal interactions," *J. Neurosci. Meth.*, vol. 83, pp. 57–72, 1998.
[38] T. A. Sears and D. Stagg, "Short-term synchronization of intercostal motoneurone activity," *J. Physiol.*, vol. 263, pp. 357–381, 1976.
[39] J. G. Semmler, K. W. Kornatz, and R. M. Enoka, "Motor Unit coherence during isometric contractions is greater in a hand muscle of older adults," *J. Neurophysiol.*, vol. 90, pp. 1346–1349, 2003.
[40] S. K. Srinivasan, *Stochastic Point Processes and their Applications*. London, U.K.: Griffin, 1974, Monograph no. 34.
[41] A. Stuart and J. K. Ord, *Kendall's Advanced Theory of Statistics. Volume 1 Distribution Theory*. London, U.K.: Arnold, 1994.
[42] T. Tateno, Y. Jimbo, and H. P. C. Robinson, "Spatio-temporal cholinergic modulation in cultured networks of rat cortical neurons: spontaneous activity," *Neuroscience*, vol. 134, pp. 425–437, 2005.
[43] T. W. Troyer and K. D. Miller, "Physiological gain leads to high ISI variability in a simple model of a cortical regular spiking cell," *Neural Comput.*, vol. 9, pp. 971–983, 1997.
[44] D. L. Tuck, "Investigation of Intercostal Neuronal Intracellular Processes and Connectivity by Signal Analysis and Computer Simulation," Ph.D. thesis, Univ. London, London, U.K., 1977.
[45] J. Ushiba, Y. Tomitaa, and Y. Masakadob, "Synchronization analysis using joint peri-stimulus time histograms for human motor units," *J. Neurosci. Meth.*, vol. 120, pp. 163–171, 2002.
[46] C. W. Vaughan and P. A. Kirkwood, "Evidence from motoneurone synchronization for disynaptic pathways in the control of inspiratory motoneurones in the cat," *J. Physiol.*, vol. 503.3, pp. 673–689, 1997.

David M. Halliday, photograph and biography not available at the time of publication.

J. R. Rosenberg, photograph and biography not available at the time of publication.

P. Breeze, photograph and biography not available at the time of publication.

B. A. Conway, photograph and biography not available at the time of publication.